ELSEVIER

Materials Science and Engineering A334 (2002) 207–214

MATERIALS SCIENCE & ENGINEERING A

www.elsevier.com/locate/msea

Evaluation of fracture toughness using small notched specimens

Baik-Woo Lee [a,*], Jae-il Jang [b], Dongil Kwon [a]

[a] *School of Materials Science and Engineering, Seoul National University, San 56-1, Shinrim-dong, Seoul 151-742, South Korea*
[b] *Frontics, Inc., Research Institute of Advanced Materials, Seoul National University, Seoul 151-742, South Korea*

Received 22 March 2001; received in revised form 27 August 2001

Abstract

As a part of small specimen testing techniques, the notched specimen technique is studied to overcome the difficulties in introducing fatigue precrack to small fracture toughness specimens. It was noted that stress triaxiality and the plastic constraint ahead of a notch root decreased with increasing notch root radius (ρ). Considering that the applied stress at the notch tip is redistributed and relaxed due to the increased plasticity, the fracture toughness obtained from notched specimens was corrected. Fracture toughness testing was conducted using an instrumented impact and a static three-point bending tester. The specimens had notch root radii which ranged from a fatigue precrack to a Charpy notch root radius of 250 μm. Fracture toughness values corrected from the results of notched specimens were very consistent with the plane strain fracture toughness obtained from precracked specimens. In addition, a limiting notch root radius (ρ_0), below which the fracture toughness was independent of ρ, was observed. To investigate this phenomenon, the fracture surface was observed with a scanning electron microscope (SEM).

Keywords: Small notched specimen; Fracture toughness; Stress redistribution; Stress relaxation; Instrumented impact test; Limiting notch root radius

1. Introduction

The critical conditions for failure or fracture can be predicted using the basic principles of fracture mechanics. Fracture mechanics is the inter-relationship between crack size, load (stress) and fracture resistance of the material. Due to this predictability, fracture toughness evaluation is one of the most important aspects used for structural integrity. Many organizations publish standardized procedures for fracture toughness measurements, including the ASTM [1] and BSI [2].

Most of the existing standards have specimen size requirements to ensure that measured values are not influenced by the specimen size. Recently, the need for small-sized specimens has arisen for several reasons, i.e. shortage of materials, limited irradiation space in nuclear plants and the requirement to quantify property gradients (e.g. irradiated components, welds). To address this need for testing of small-sized specimens, many studies have been taken to develop testing technologies for small-volume specimens [3–5]. There are, however, many difficulties with fracture toughness measurement using currently accepted small specimen testing techniques. The problem is mainly due to the difficulty in introducing a fatigue precrack into a small-sized specimen. The requirement to introduce a precrack is necessary when evaluating fracture toughness based on fracture mechanics.

The primary objective of this study was to check if an easily machined small notched specimen would be an acceptable alternative for evaluating fracture toughness. The notch effects on fracture toughness were divided into stress redistribution and stress relaxation effects and they were corrected. Corrected values of the notched specimens' fracture toughness were compared with those obtained from precracked specimens.

* Corresponding author.
E-mail address: leebew@snu.ac.kr (B.-W. Lee).

0921-5093/02/$ - see front matter
PII: S0921-5093(01)01804-4

2. Theoretical analysis of notch effect

2.1. Stress triaxiality of notched specimens

The prime effects of a notch including a crack are introducing a stress concentration and producing a triaxial stress at the notch/crack tip. If the specimen embedding notch/crack is subjected to loading as shown in Fig. 1, then high longitudinal stress (σ_{yy}) at the notch/crack tip causes the specimen to extend elastically and to contract laterally due to the Poisson effect. This contraction is greatest near the notch/crack tip where σ_{yy} is the highest. The longitudinal stress (σ_{yy}) falls off rapidly away from the notch/crack tip and this region does not tend to contract. As the area away from the notch/crack tip tends to maintain its original dimensions while the area adjacent to the notch/crack tip is contracting, the lateral stresses (σ_{xx} and σ_{zz}) exist near the notch/crack tip to prevent contraction and maintain continuity. A triaxial state of stress is therefore developed around the crack/notch tip. The existence of these lateral stresses raises the average value of σ_{yy} at which point yielding begins. The triaxial stress state makes it more difficult to spread the yielding zone at the notch/crack tip.

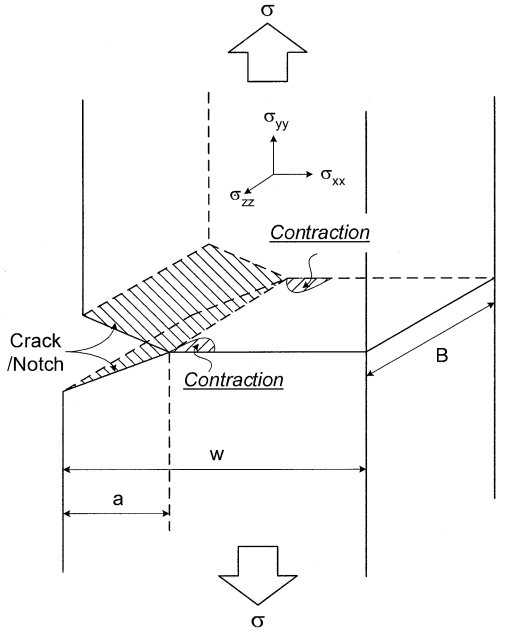

Fig. 1. Schematic illustration of the transverse contraction that occurs ahead of a crack/notch.

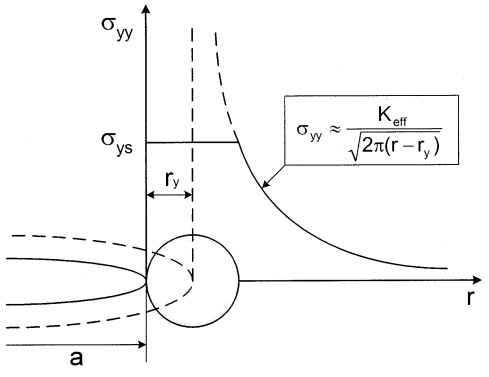

Fig. 2. Correction of Irwin plastic zone.

Since σ_{yy} ahead of a notch decreases with increasing notch root radius, the stress triaxiality also decreases. This means that the plastic zone size ahead of the notch increases with notch root radius (ρ). The fracture toughness of a notched specimen can be evaluated by considering the increased plastic zone size when compared to the precracked specimen. Infinite stress at the crack tip, which is assumed in linear elastic fracture mechanics, should be reanalyzed as the inelastic region grows at the notch tip. Also, correction of the stress relaxation effect caused by this plastic deformation is required.

2.2. Correction of stress redistribution effect

Fracture mechanics assumes the existence of very sharp cracks in continuous solids. Linear elastic stress analysis predicts the presence of infinite stresses at the crack tip. In real materials, the yielding occurs at the crack tip. Due to this yielding, the σ_{yy} cannot exceed the material's uniaxial yield strength (σ_{ys}) for plane stress condition, and three times the yield strength for plane strain condition. This means that the infinite stress must be redistributed to satisfy force equilibrium when yielding occurs.

As plastic deformation also occurs at the notch tip, the stress redistribution at the notch tip was considered. The stress redistribution effect can be corrected by applying the Irwin approach [6]. He corrected the stress redistribution effect on fracture toughness by defining an effective crack length (a_{eff}). The effective crack length is defined as the sum of the original crack length and plastic zone size, as shown in Fig. 2.

$$a_{eff} = a + r_y \tag{1}$$

where a is the original crack length (here, equivalent to notch depth) and r_y is plastic zone size; r_y is determined according to the stress state at the crack tip.

In case of plane stress condition

$$r_y = \frac{1}{2\pi}\left(\frac{K_I}{\sigma_{ys}}\right)^2 \tag{2a}$$

In case of plane strain condition

$$r_y = \frac{1}{6\pi}\left(\frac{K_I}{\sigma_{ys}}\right)^2 \tag{2b}$$

where K_I is the stress intensity factor and σ_{ys} the yield strength.

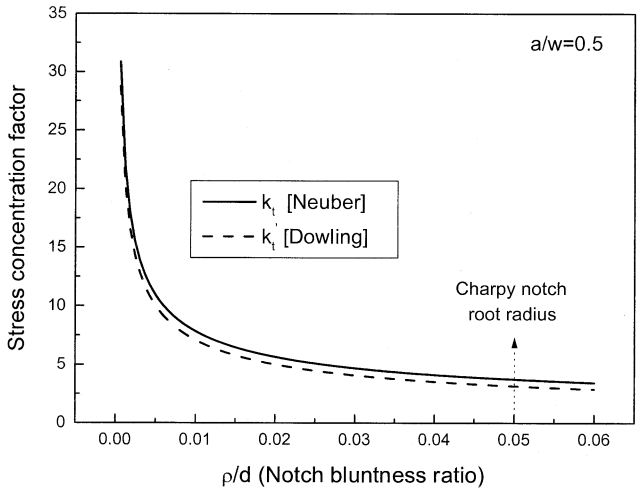

Fig. 3. Stress concentration factors as a function of ρ/d ($d = 5$ mm).

Since the notch tip is a free surface and carries no stress on that surface (plane stress state), the effective crack length for notched specimens is determined by inserting Eq. (2a) into Eq. (1).

The effective fracture toughness ($(K_I)_{eff}$), for the case where the stress redistribution effect is corrected, can be obtained by inserting the effective crack length into the stress intensity factor as follows:

$$(K_I)_{eff} = \lambda(a_{eff})\sigma_{nom}\sqrt{\pi a_{eff}} \tag{3}$$

where $\lambda(a_{eff})$ is a parameter that depends on the specimen and crack geometry and σ_{nom} is nominal stress.

The Irwin approach does not consider the stress relaxation by excessive plastic deformation at the notch tip. From this observation, the stress relaxation effect should be also considered.

2.3. Correction of stress relaxation effect

The stress concentration factor was considered as a possible parameter to be used for correcting the stress relaxation effect as it can control deformation and fracture below the notch. The stress concentration factor in linear elastic materials is described as the ratio of the maximum stress to the nominal stress based on the net section.

$$k_t = \frac{\sigma_{max,tip}}{\sigma_{nom}} \tag{4}$$

Substituting Eq. (4) into the nominal stress in Eq. (3), the fracture toughness of the notched specimen without stress relaxation can be represented by the stress concentration factor:

$$K_I = \lambda \frac{\sigma_{max,tip}}{k_t}\sqrt{\pi a} \tag{5}$$

k_t is the stress concentration factor when the elastic stress state is maintained at the notch tip and stress relaxation does not occur. This can be calculated from Neuber's nomograph [7].

$$k_t = 1 + \frac{(\alpha_{fk}-1)(\alpha_{tk}-1)}{\sqrt{(\alpha_{fk}-1)^2(\alpha_{tk}-1)^2}} \tag{6}$$

where both α_{fk} and α_{tk} are a function of a/ρ and d/ρ (d: ligament length).

The fracture toughness, which should consider the stress relaxation effect, can also be represented as shown in Eq. (5)

$$K_I' = \lambda \frac{\sigma'_{max,tip}}{k_t'}\sqrt{\pi a} \tag{7}$$

where $\sigma'_{max,tip}$ is the maximum stress and k_t' is the stress concentration factor at this time. Dowling suggested a stress concentration factor in the notched specimen using a stress intensity factor that was calculated for the hypothetical case where the notch is collapsed to form a crack of the same major dimension [8]:

$$k_t' = \frac{2K_I}{\sigma_{nom}\sqrt{\pi\rho}} \tag{8}$$

Fig. 3 shows the elastic stress concentration factor based on Neuber's and Dowling's method as a function of ρ/d. It can be seen that k_t' becomes smaller than k_t as ρ increases. The stress intensity factor in Eq. (8), which is only effective under linear elastic state, is suspected to deviate from the linear elastic behavior. Plastic deformation will occur to the extent of deviation from the linear elastic state, so that the stress will become relaxed. Since both $\sigma_{max,tip}$ in Eq. (5) and $\sigma'_{max,tip}$ in Eq. (7) must reach the critical fracture strength of σ_f to initiate fracture, the stress relaxation effect can be corrected using the ratio of stress concentration factors from Eqs. (5) and (7).

$$K_I = \frac{k_t'}{k_t}K_I' \tag{9}$$

Finally, by putting the effective fracture toughness into K_I' in Eq. (9), the fracture toughness, which corrected both stress redistribution and stress relaxation effects, can be obtained.

3. Experimental procedures

The material used in this study was SA 508 class 3 steel, which is the type of material used for constructing nuclear pressure vessels in Korea. This material's chemical composition and mechanical properties are given in Table 1. Standard size ($10 \times 10 \times 55$ mm^3) Charpy specimens were used for both dynamic and static fracture toughness tests. Notches with root radii ranging from 60 to 280 μm were machined mechanically, as shown in Fig. 4. Their root radii were measured with an optical microscope. The ratio of notch depth to the specimen width (a/w) was set at 0.5 for all specimens. A precracked

specimen was also prepared to obtain the plane strain fracture toughness. Fatigue precrack was made according to the ASTM E399 method [2].

Dynamic fracture toughness testing was performed using a pendulum instrumented impact tester (Tinius–Olsen Model) with 406 J capacity at a loading rate of 1.27 m s^{-1}. The tup of the impact hammer was instrumented with a load cell (strain gauge-type) to record the loading applied to the specimens as a function of time. A light velocity sensor was used to measure impact velocity and calculate displacement. The output signals from the load cell and the velocity sensor were passed through an amplifier and then to a data acquisition system. The acquisition system receives output signals at high speed (5 MHz) and resolution (12 bits) and also has a large memory (16 MB).

Static fracture toughness testing was performed using 10 ton capacity universal tester (Instron Model 5582). The specimens were loaded in three-point bending at a crosshead speed of 0.5 mm min^{-1}.

All the fracture toughness tests were conducted at liquid nitrogen temperature (77 K). For low temperature testing, dynamic tests were conducted according to ASTM E23 [9] with all the testing procedures being completed in less than 5 s, after holding the specimens in a liquid medium for at least 5 min. For the static test, the specimens were tested according to the ASTM E399 test method, in a constant temperature bath capable of controlling to ± 1 K. After testing, the fracture surface was observed by scanning electron microscope (SEM).

4. Results and discussion

Figs. 5a and 6a show the fracture toughness obtained from the load–displacement curve under dynamic and static loading state. Plane strain fracture toughness values were obtained from precracked specimens, satisfying plane strain conditions, under each loading state. The values for dynamic (K_{ID}) and static (K_{IC}) loading were

Table 1
Chemical compositions and mechanical properties of materials used in this study

(a) Chemical compositions:										
Element	C	Mn	P	Si	Ni	Cr	Mo	V	Cu	Al
Chemical composition (wt.%)	0.21	1.36	0.007	0.24	0.92	0.21	0.49	0.005	0.03	0.022
(b) Mechanical properties:										
Temperature	Yield strength (MPa)	Tensile strength (MPa)								
Room temperature	457	602								
77 K	918	968								

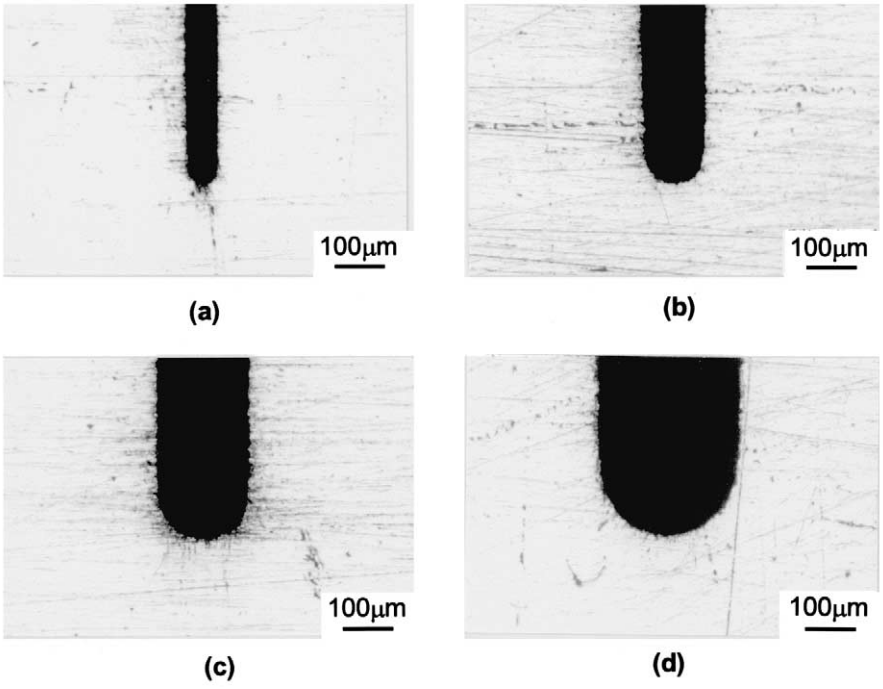

Fig. 4. Microviews of various notch root radius specimens: (a) $\rho = 60$ μm; (b) $\rho = 120$ μm; (c) $\rho = 180$ μm; and (d) $\rho = 280$ μm.

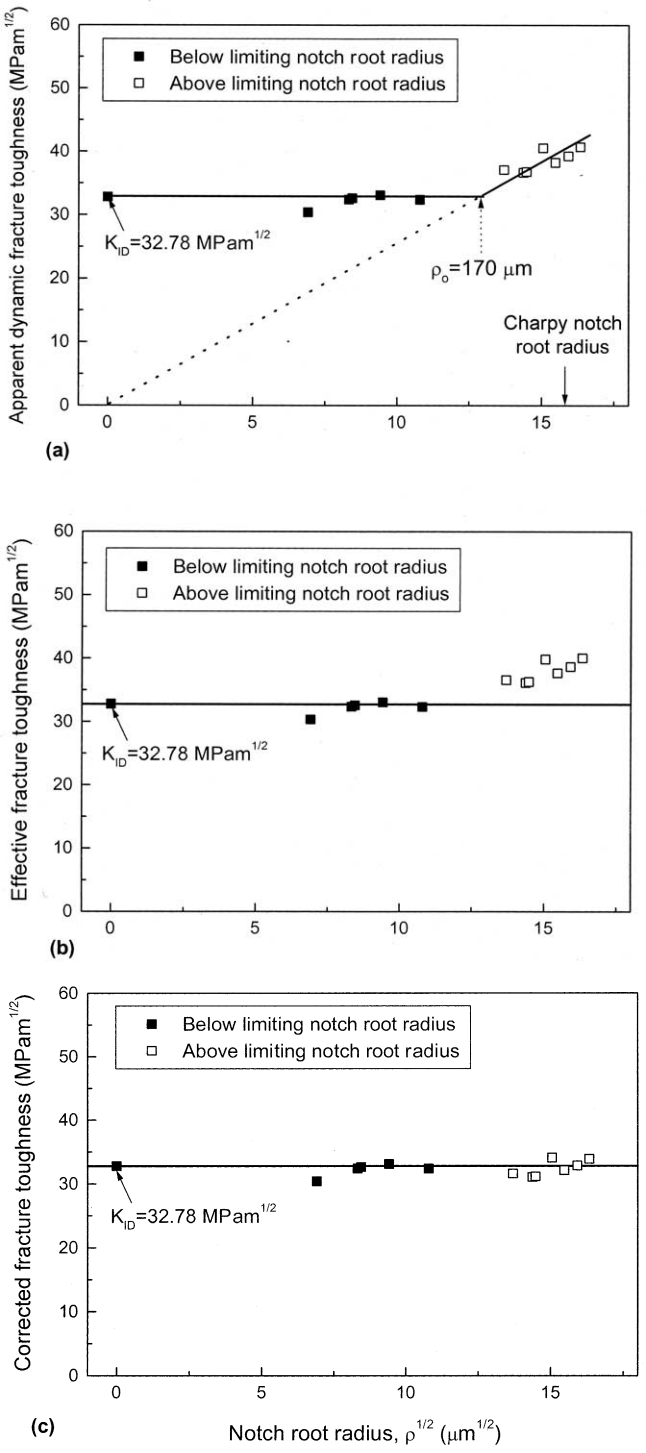

Fig. 5. Fracture toughness as a function of the square root of notch root radius ($\rho^{1/2}$) under dynamic loading: (a) apparent; (b) effective; and (c) notch effects corrected.

32.78 MPa m$^{1/2}$ and 46.70 MPa m$^{1/2}$, respectively. Apparent fracture toughness values, which are obtained from notched specimens, are also shown as a function of the square root of ρ. There appears to be a limiting notch root radius (ρ_0) below which the fracture toughness is independent of ρ. Above ρ_0, apparent fracture toughness values are directly proportional to the square root of ρ. This observation is also shown in other previous researches [10–12]. The decrease in stress triaxiality with increasing ρ was confirmed to cause a decrease in the stress that would initiate fracture. The conclusion from this is that the fracture toughness increases with ρ. The ρ_0 phenomena will be described later.

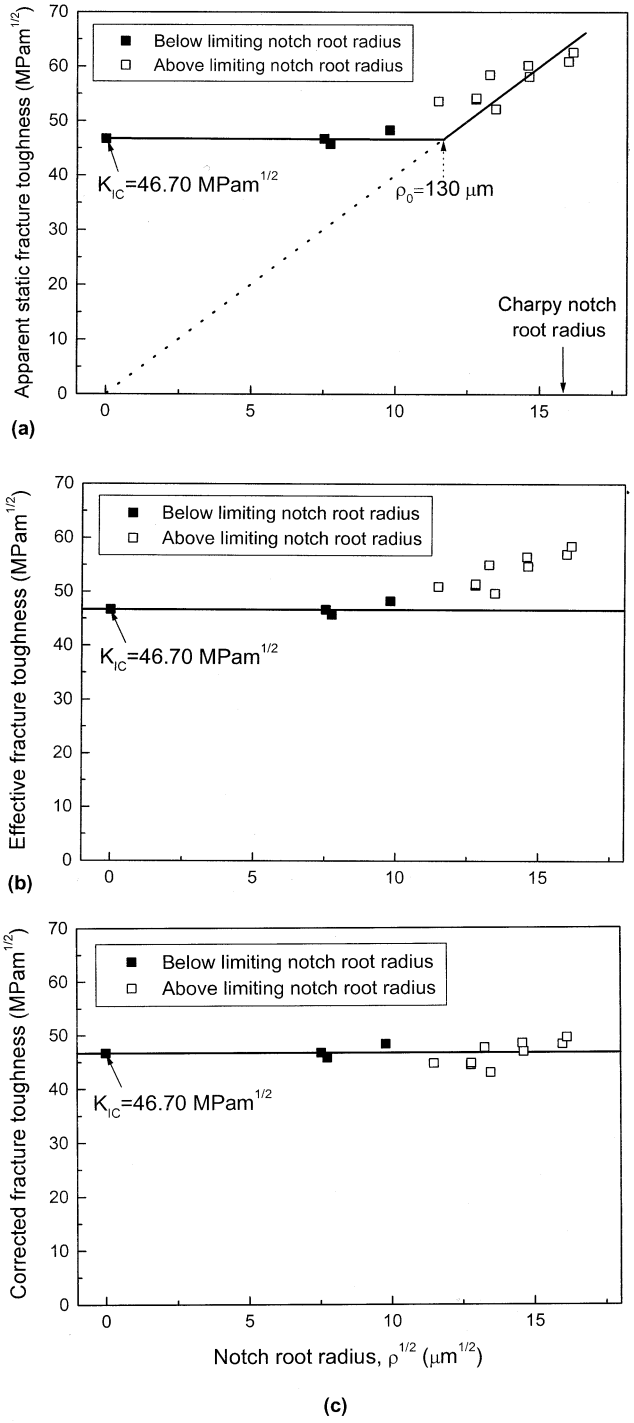

Fig. 6. Fracture toughness as a function of the square root of notch root radius ($\rho^{1/2}$) under static loading: (a) apparent; (b) effective; and (c) notch effects corrected.

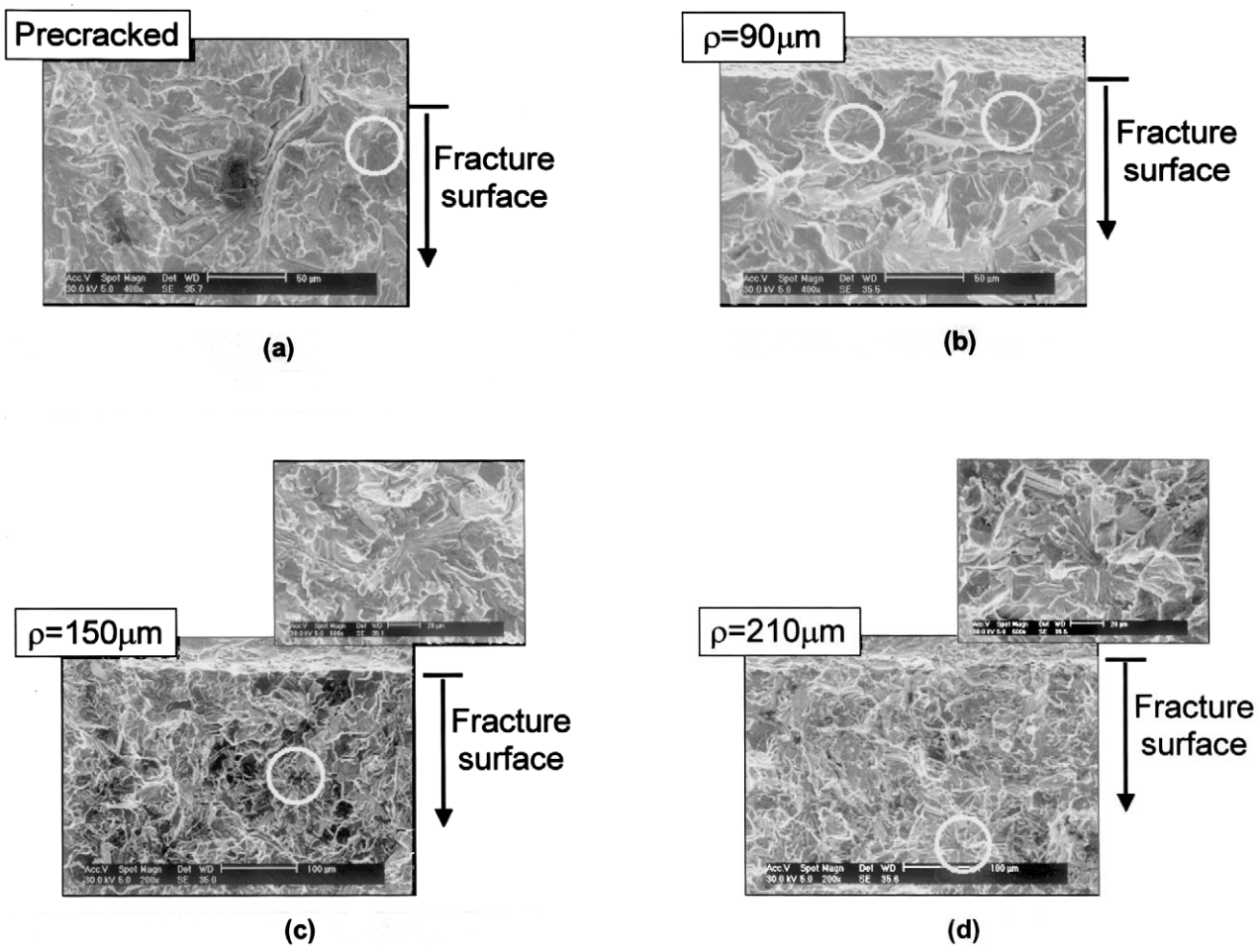

Fig. 7. SEM micrographs showing fracture origin locations: (a) precracked; (b) $\rho = 90$ μm; (c) $\rho = 150$ μm; and (d) $\rho = 210$ μm.

For apparent fracture toughness above ρ_0, stress redistribution effect was corrected by using Eq. (3). Figs. 5b and 6b show the effective fracture toughness obtained by the correction of stress redistribution effect under dynamic and static loading state. They show that notch effects were partially corrected. The correction of stress redistribution has a small effect for the precracked specimens [13] while it has considerable effect for the notched specimens that are shown in the figures. Since the notched specimens have larger plasticity at the notch tip than the precracked specimen, the stress redistribution becomes important. But, there is still a significant difference between the effective fracture toughness and plane strain fracture toughness. Because of this difference, the stress relaxation effect was also considered.

For effective fracture toughness, the stress relaxation effect was corrected by using Eq. (9). Figs. 5c and 6c show the fracture toughness obtained by the correction of both stress redistribution and stress relaxation effects under dynamic and static loading, respectively. Fracture toughness values obtained by the correction of both notch effects were consistent with the plane strain fracture toughness obtained from the precracked specimens when under each loading state. It was confirmed that notch effects were reasonably analyzed and corrected.

Apparent fracture toughness is independent of ρ when it is below ρ_0. This apparent fracture toughness has the same value as plane strain fracture toughness when it is measured in precracked specimens, as shown in Figs. 5 and 6. Ritchie and Swanson have also observed the existence of ρ_0 [11,12]. Their studies only suggested that it would be related with some microstructural features. In this study, ρ_0 is discussed from observing fracture surfaces after testing.

Fig. 7 shows the scanning electron micrographs for fracture surfaces after static fracture testing. Cleavage fracture occurred in all the specimens. For cleavage fracture to initiate, the stress ahead of the crack/notch tip must exceed σ_f over a characteristic distance (x_c). σ_f is determined by intrinsic variables such as microstructure and extrinsic variables such as temperature and strain rate. Characteristic distance (x_c) represents the

minimum distance from the crack/notch tip which must be sampled ahead of the crack/notch tip to find a fracture initiation site, such as second phase particle, slip band or twin band [10,11,14]. The materials used in this study have the microstructure of bainitic ferrite lath created by a quenching and tempering process, as shown in Fig. 8. In the quenched and tempered steels, cleavage fracture usually initiates at second phase particle such as carbide or an inclusion [11,14].

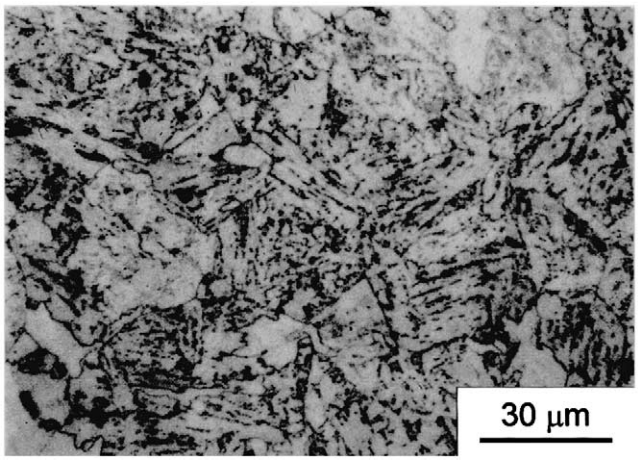

Fig. 8. An optical micrograph of SA 508 class 3 steel.

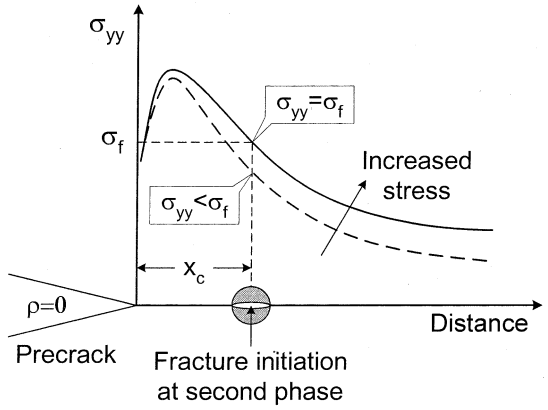

Fig. 9. Schematic of cleavage fracture initiation at second phase particle ahead of: (a) a precrack; and (b) a limiting notch root.

As shown in Fig. 7a and b, fracture origin locations (white circle in figures) are constant up to about 30 μm below ρ_0, while they move away from the notch tip with ρ above ρ_0. These observations show that fracture initiation in the notched specimens below ρ_0, including the precracked specimen, occurred at the same fracture initiation site under the same applied stress. Thus, the specimens have the same fracture toughness. This also means that the stress redistribution and stress relaxation are minimal below ρ_0.

Precracked specimens and notched specimens below ρ_0 can fail under the same applied stress, even though the stress concentration is higher in the precracked specimens than in the notched. The stress at the crack tip in a precracked specimen can easily reach σ_f due to high stress concentration, even when a stress that is lower than which would fracture the notched specimens below ρ_0 is applied. However, the precracked specimen may not fail, since the stress gradient at the crack tip is so steep that the stress at the fracture initiation site cannot reach σ_f (the dotted line in Fig. 9a). To initiate the fracture, the applied stress should increase until the stress at the fracture initiation site reaches σ_f (the solid line in Fig. 9a). An applied stress of this magnitude can also fracture the notched specimens below ρ_0, in spite of the lower stress concentration around the notch. The stress redistribution and stress relaxation effects are relatively small even with increasing ρ below ρ_0, as mentioned above. The free surface of a notch produces triaxial stress far from the notch tip (that is, near the fracture initiation site). Hence, the stress can easily reach σ_f at the fracture initiation site, as shown in Fig. 9b.

The specimen above ρ_0 experiences stress redistribution and stress relaxation effects at the notch tip. This causes the fracture initiation site to move away from the notch tip (Fig. 7c and d).

The ρ_0s are 130 μm for static loading state and 170 μm for dynamic loading state. A high loading rate tends to elevate the flow stress of the material. The elevated flow stress compensates the decrease in stress triaxiality ahead of a notch. The specimens with larger ρ can be easily fractured without stress redistribution and stress relaxation effects while the loading rate increases. Thus, ρ_0 is larger for dynamic loading state than for static loading.

The magnitude of ρ_0 is suspected to depend on the ability to concentrate stress ahead of a notch and the site of local inhomogeneity to initiate fracture.

5. Conclusions

Using small notched specimens, the fracture toughness could be evaluated from both instrumented impact and static three-point bending test. This use of small notched specimens is expected to overcome the difficulties caused by introducing precrack to small fracture toughness-specimens. (1) The stress redistribution effect of notch effects was corrected from the effective fracture toughness. This was calculated by substituting an effective crack length (i.e. the sum of original crack length and plastic zone size), rather than by using the original crack length. (2) The stress relaxation effect of notch effects was corrected by the elastic stress concentration factors' ratio under elastic stress state to stress-relaxed state. (3) The corrected fracture toughness values of notched specimens were consistent with plane strain fracture toughness obtained from precracked specimens. (4) There appeared to be a limiting notch root radius (ρ_0) below which the fracture toughness was independent of ρ. It is because the specimens below ρ_0 failed at the same fracture initiation site under the same applied stress.

Acknowledgements

This work was supported by the Korean Ministry of Science and Technology as a part of the National Research Laboratory Program.

References

[1] ASTM Standard E399, Standard Test Method for Plane-Strain Fracture Toughness of Metallic Materials, American Society for Testing and Materials, Philadelphia, 1995.
[2] BS7448, Fracture Mechanics Toughness Tests, British Standards Institution, London, 1997.
[3] G.E. Lucas, Metall. Mater. Trans. A 21 (1990) 1105.
[4] P. Jung, A. Hishinuma, G.E. Lucas, H. Ullmaier, J. Nucl. Mater. 232 (1996) 186.
[5] R.A. Wullaert, W.L. Server, Nucl. Eng. Des. 57 (1980) 153.
[6] G.R. Irwin, Proceedings of 7th Sagamore Ordnance Materials Research Conference on Mechanics and Metals Behavior of Sheet Material, Racquette Lake, NY, August, 1960, Syracuse University Publishers, NY, 1960, p. 463.
[7] H. Neuber, Theorie der ebenen Kerbwirkung, Kerbspannungslehre, Verlag von Julius Springer, Berlin, 1958, pp. 27–68.
[8] N.E. Dowling, Eng. Fract. Mech. 20 (1984) 569.
[9] ASTM Standard E23, Standard Test Methods for Notched Bar Impact Testing of Metallic Materials, American Society for Testing and Materials, Philadelphia, 1996.
[10] T.R. Wilshaw, C.A. Rau, A.S. Tetelman, Eng. Frac. Mech. 1 (1968) 191.
[11] R.O. Ritche, B. Francis, W.L. Server, Metall. Mater. Trans. A 7 (1976) 831.
[12] R.E. Swanson, A.W. Thompson, I.M. Bernstein, Metall. Mater. Trans. A 17 (1986) 1633.
[13] G.E. Dieter, Mechanical Metallurgy, McGraw-Hill, London, 1988, p. 361.
[14] T.L. Anderson, Fracture Mechanics Fundamental and Applications, CRC Press, Florida, 1995, p. 285.